Research Article | Vol. 25, No. 6 | 20 Mar 2017 | OPTICS EXPRESS 6883

Optics EXPRESS

Near-field spectral properties of coupled plasmonic nanoparticle arrays

HAN YU,[1] QUAN SUN,[1] JINGHUAN YANG,[2] KOSEI UENO,[1] TOMOYA OSHIKIRI,[1] ATSUSHI KUBO,[3] YASUTAKA MATSUO,[1] QIHUANG GONG,[2,4] AND HIROAKI MISAWA[1,5,*]

[1]*Research Institute for Electronic Science, Hokkaido University, Sapporo 001-0021, Japan*
[2]*State Key Laboratory for Mesoscopic Physics and Department of Physics, Peking University, Beijing 100871, China*
[3]*Institute of Physics, University of Tsukuba, Tsukuba 305-8571, Japan*
[4]*Collaborative Innovation Center of Quantum Matter, Beijing 100871, China*
[5]*Department of Applied Chemistry & Institute of Molecular Science, National Chiao Tung University, Hsinchu 30010, Taiwan*
[*]*misawa@es.hokudai.ac.jp*

Abstract: We investigated the grating effect in complex gold dolmen structures, in which multiple plasmon modes are present due to plasmon hybridization, experimentally from both the far field and the near field. In particular, the near-field properties were investigated using photoemission electron microscopy, and it was demonstrated that two hybridized plasmon modes on the dolmen structures could be influenced by the grating effect. For comparison, we also investigated the grating effect in arrays of simple nanoblocks and heptamer structures, which were supposed to support a strong bright plasmon mode and a strong dark plasmon mode, respectively, in the near field. We found that the spectral responses of the two hybridized modes on the dolmen structures as the pitch size changed evolved in a manner similar to that of the bright dipole mode on the nanoblocks, whereas the dark mode on the heptamer structures is less sensitive to the pitch size.

OCIS codes: (240.6680) Surface plasmons; (240.6675) Surface photoemission and photoelectron spectroscopy; (190.4180) Multiphoton processes; (180.4243) Near-field microscopy; (320.7090) Ultrafast lasers.

References and links

1. Y. Zhang, Y. R. Zhen, O. Neumann, J. K. Day, P. Nordlander, and N. J. Halas, "Coherent anti-Stokes Raman scattering with single-molecule sensitivity using a plasmonic Fano resonance," Nat. Commun. **5**, 4424 (2014).
2. P. K. Jain, X. Huang, I. H. El-Sayed, and M. A. El-Sayed, "Noble metals on the nanoscale: optical and photothermal properties and some applications in imaging, sensing, biology, and medicine," Acc. Chem. Res. **41**(12), 1578–1586 (2008).
3. S. Gao, K. Ueno, and H. Misawa, "Plasmonic antenna effects on photochemical reactions," Acc. Chem. Res. **44**(4), 251–260 (2011).
4. K. Ueno and H. Misawa, "Plasmon-enhanced photocurrent generation and water oxidation from visible to near-infrared wavelengths," NPG Asia Mater. **5**(9), e61 (2013).
5. T. Oshikiri, K. Ueno, and H. Misawa, "Selective dinitrogen conversion to ammonia using water and visible light via plasmon-induced charge separation," Angew. Chem. Int. Ed. Engl. **55**(12), 3942–3946 (2016).
6. Y. Zhong, K. Ueno, Y. Mori, X. Shi, T. Oshikiri, K. Murakoshi, H. Inoue, and H. Misawa, "Plasmon-assisted water splitting using two sides of the same $SrTiO_3$ single-crystal substrate: conversion of visible light to chemical energy," Angew. Chem. Int. Ed. Engl. **53**(39), 10350–10354 (2014).
7. E. Prodan, C. Radloff, N. J. Halas, and P. Nordlander, "A hybridization model for the plasmon response of complex nanostructures," Science **302**(5644), 419–422 (2003).
8. Y. Sonnefraud, A. L. Koh, D. W. McComb, and S. A. Maier, "Nanoplasmonics: engineering and observation of localized plasmon modes," Laser Photonics Rev. **6**(3), 277–295 (2012).
9. T. Coenen, D. T. Schoen, S. A. Mann, S. R. K. Rodriguez, B. J. M. Brenny, A. Polman, and M. L. Brongersma, "Nanoscale spatial coherent control over the modal excitation of a coupled plasmonic resonator system," Nano Lett. **15**(11), 7666–7670 (2015).
10. B. Luk'yanchuk, N. I. Zheludev, S. A. Maier, N. J. Halas, P. Nordlander, H. Giessen, and C. T. Chong, "The Fano resonance in plasmonic nanostructures and metamaterials," Nat. Mater. **9**(9), 707–715 (2010).

#285678 https://doi.org/10.1364/OE.25.006883
Journal © 2017 Received 26 Jan 2017; revised 28 Feb 2017; accepted 13 Mar 2017; published 15 Mar 2017

Optics EXPRESS

11. N. Verellen, Y. Sonnefraud, H. Sobhani, F. Hao, V. V. Moshchalkov, P. Van Dorpe, P. Nordlander, and S. A. Maier, "Fano resonances in individual coherent plasmonic nanocavities," Nano Lett. **9**(4), 1663–1667 (2009).
12. C. Yan and O. J. F. Martin, "Periodicity-induced symmetry breaking in a Fano lattice: hybridization and tight-binding regimes," ACS Nano **8**(11), 11860–11868 (2014).
13. J. Ye, F. Wen, H. Sobhani, J. B. Lassiter, P. Van Dorpe, P. Nordlander, and N. J. Halas, "Plasmonic nanoclusters: near field properties of the Fano resonance interrogated with SERS," Nano Lett. **12**(3), 1660–1667 (2012).
14. J. B. Lassiter, H. Sobhani, J. A. Fan, J. Kundu, F. Capasso, P. Nordlander, and N. J. Halas, "Fano resonances in plasmonic nanoclusters: geometrical and chemical tunability," Nano Lett. **10**(8), 3184–3189 (2010).
15. B. Gallinet and O. J. F. Martin, "Relation between near-field and far-field properties of plasmonic Fano resonances," Opt. Express **19**(22), 22167–22175 (2011).
16. M. Hentschel, M. Saliba, R. Vogelgesang, H. Giessen, A. P. Alivisatos, and N. Liu, "Transition from isolated to collective modes in plasmonic oligomers," Nano Lett. **10**(7), 2721–2726 (2010).
17. M. Frimmer, T. Coenen, and A. F. Koenderink, "Signature of a Fano resonance in a plasmonic metamolecule's local density of optical states," Phys. Rev. Lett. **108**(7), 077404 (2012).
18. M. Meier, P. F. Liao, and A. Wokaun, "Enhanced fields on rough surfaces - dipolar interactions among particles of sizes exceeding the Rayleigh limit," J. Opt. Soc. Am. B **2**(6), 931–949 (1985).
19. B. Lamprecht, G. Schider, R. T. Lechner, H. Ditlbacher, J. R. Krenn, A. Leitner, and F. R. Aussenegg, "Metal nanoparticle gratings: influence of dipolar particle interaction on the plasmon resonance," Phys. Rev. Lett. **84**(20), 4721–4724 (2000).
20. N. Félidj, G. Laurent, J. Aubard, G. Lévi, A. Hohenau, J. R. Krenn, and F. R. Aussenegg, "Grating-induced plasmon mode in gold nanoparticle arrays," J. Chem. Phys. **123**(22), 221103 (2005).
21. A. O. Pinchuk and G. C. Schatz, "Nanoparticle optical properties: far- and near-field electrodynamic coupling in a chain of silver spherical nanoparticles," Mater. Sci. Eng. B **149**(3), 251–258 (2008).
22. C. L. Haynes, A. D. McFarland, L. L. Zhao, R. P. Van Duyne, G. C. Schatz, L. Gunnarsson, J. Prikulis, B. Kasemo, and M. Kall, "Nanoparticle optics: the importance of radiative dipole coupling in two-dimensional nanoparticle arrays," J. Phys. Chem. B **107**(30), 7337–7342 (2003).
23. N. J. Halas, S. Lal, W. S. Chang, S. Link, and P. Nordlander, "Plasmons in strongly coupled metallic nanostructures," Chem. Rev. **111**(6), 3913–3961 (2011).
24. H. Yu, Q. Sun, K. Ueno, T. Oshikiri, A. Kubo, Y. Matsuo, and H. Misawa, "Exploring coupled plasmonic nanostructures in the near field by photoemission electron microscopy," ACS Nano **10**(11), 10373–10381 (2016).
25. Q. Sun, H. Yu, K. Ueno, A. Kubo, Y. Matsuo, and H. Misawa, "Dissecting the few-femtosecond dephasing time of dipole and quadrupole modes in gold nanoparticles using polarized photoemission electron microscopy," ACS Nano **10**(3), 3835–3842 (2016).
26. Q. Sun, K. Ueno, H. Yu, A. Kubo, Y. Matsuo, and H. Misawa, "Direct imaging of the near field and dynamics of surface plasmon resonance on gold nanostructures using photoemission electron microscopy," Light Sci. Appl. **2**(12), e118 (2013).
27. F. Schertz, M. Schmelzeisen, R. Mohammadi, M. Kreiter, H. J. Elmers, and G. Schönhense, "Near field of strongly coupled plasmons: uncovering dark modes," Nano Lett. **12**(4), 1885–1890 (2012).
28. A. Kubo, K. Onda, H. Petek, Z. Sun, Y. S. Jung, and H. K. Kim, "Femtosecond imaging of surface plasmon dynamics in a nanostructured silver film," Nano Lett. **5**(6), 1123–1127 (2005).
29. P. Melchior, D. Kilbane, E. J. Vesseur, A. Polman, and M. Aeschlimann, "Photoelectron imaging of modal interference in plasmonic whispering gallery cavities," Opt. Express **23**(25), 31619–31626 (2015).
30. R. C. Word and R. Könenkamp, "Mode structure of planar optical antennas on dielectric substrates," Opt. Express **24**(16), 18727–18738 (2016).
31. B. Y. Ji, J. Qin, H. Y. Tao, Z. Q. Hao, and J. Q. Lin, "Subwavelength imaging and control of ultrafast optical near-field under resonant- and off-resonant excitation of bowtie nanostructures," New J. Phys. **18**(9), 093046 (2016).
32. P. B. Johnson and R. W. Christy, "Optical constants of noble metals," Phys. Rev. B **6**(12), 4370–4379 (1972).

1. Introduction

Over the past few decades, localized surface plasmon resonances (LSPRs) supported on metallic nanoparticles (NPs) have attracted significant research interest due to their abundant optical properties and broad range of applications in various fields, including surface-enhanced Raman scattering [1], sensing [2], plasmon-assisted photochemical reactions [3], photocurrent generation [4], and artificial photosynthesis [5, 6]. In terms of the optical properties of LSPRs, metallic NPs exhibit intense light absorption and scattering in the far field that depends strongly on the size, shape, and dielectric function of the metal and the dielectric constant of the surrounding medium [2]. Furthermore, complex metallic NP aggregates can induce plasmon coupling that exhibits some striking properties, such as plasmon hybridization [7, 8] and Fano resonance [9–17].

Optics EXPRESS

The optical properties of metallic NPs in a regular two-dimensional (2D) array can be different from those of individual NPs, and they can be influenced by the pitch size. In a metallic NP array, two types of interaction between nearby NPs can be distinguished, namely, near-field coupling and far-field coupling, for different pitch sizes (for a single NP array, this can also refer to the inter-particle distance, d). On one hand, when d is much smaller than the NP size, near-field coupling with d^{-3} dependence dominates, as a result of interactions between adjacent NPs due to the short range of the electromagnetic field within several tens of nanometers. On the other hand, when d is comparable to the NP size and the LSPR wavelength, far-field coupling with d^{-1} dependence dominates as a result of long-range dipole-dipole interactions in the scattered light field. Near- and far-field coupling can normally be separated by changing the pitch size of the ensemble of metallic NPs. For arrays formed from single metallic NPs, such as arrays of nanoblocks, nanodisks, and nanorods, the effects of near- and far-field coupling have been investigated intensively, and in the far-field coupling regime the grating effect plays an important role in determining the plasmonic properties [18–23]. When the diffraction order is evanescent, that is, the diffracting light propagates along the plane of the array, the local optical fields in the plane become large resulted from an almost in-phase addition of the scattered light field of neighboring particles. This can result in the shift of the plasmon resonance. Additionally, when the grating order is switched between the evanescent and radiating, the plasmon damping property is also modified due to the change in the radiating loss [19]. This grating effect should also alter the near-field plasmonic properties, since the far field and the near field are influenced by each other. However, when complex NP aggregates are arranged in regular arrays, the near- and far-field plasmon coupling becomes more complex because near-field coupling already plays an important role in the plasmonic properties of even a single aggregate unit. Furthermore, the effects of far- and near-field coupling on the plasmonic properties have been investigated, mainly through far-field spectroscopic measurements. Near-field measurements will provide new insights into plasmon coupling in complex metallic NP arrays, but they are still lacking. Such near-field measurements of plasmonic nanostructures can be made using multiphoton photoemission electron microscopy (PEEM), which has been used to investigate the near-field properties of not only simple NPs but also complex aggregated nanostructures [24–31].

In this study, we investigated far-field coupling, especially the grating effect, in arrays of complex coupled plasmonic nanostructures through near-field measurements using PEEM. In particular, we first investigated gold (Au) dolmen structures, which have been largely reported to exhibit Fano resonances [9–12, 15]. Very recently, we clarified that in the dolmen structures, plasmon hybridization, not Fano resonance dominates the plasmon coupling using near-field measurements based on PEEM [24]. We also spectrally and spatially resolved the bonding and anti-bonding hybridized modes in the near field. However, in that previous study, the pitch size was fixed at 1000 nm. In this study, we further investigated how the pitch size affects the two hybridized modes in far-field coupling regime. We observed the spectral shifts of the bonding and anti-bonding modes while varying the pitch size. More interestingly, we found that the anti-bonding mode was dramatically suppressed when the pitch size was similar to the grating constant. These results can be explained using the grating effect. For comparison, the grating effects for simple nanoblock and plasmonic nano heptamer structures were investigated to better understand the mechanism.

2. Methods

Various Au nanostructures were fabricated on indium tin oxide (ITO) coated glass substrate using electron beam lithography (EBL) and metal sputtering. The fabrication procedure used in this study was similar to the process described in our previous works [24–26]. Here, a high-resolution EBL system (ELS-F130HM, Elionix) operated at 130 kV was used. The EBL was conducted at a current of 50 pA. After the development, a 2-nm-thick titanium adhesive layer was deposited first; it was followed by 30 nm-thick Au film deposited *via* sputtering (MPS-

Optics EXPRESS

4000, ULVAC). Lift-off was performed by successively immersing the sample in anisole, acetone, methanol, and ultra-pure water in an ultrasonic bath. Morphologies were analyzed using field-emission scanning electron microscopy (SEM) (JSM-6700FT, JEOL). Far-field spectral properties were analyzed using Fourier transform infrared (FT-IR) equipped with an infrared microscope (FT/IR-6000TM-M, JASCO).

The photoemission electron microscope used in this study was a PEEM-III equipped with an energy analyzer (Elmitec GmbH). We used two light beams as excitation sources for the PEEM. One beam consisted of UV light from a mercury lamp (unpolarized CW light with a cutoff energy of 4.9 eV); it was used to characterize the morphologies of metallic NPs. The other was a Ti:sapphire femtosecond laser that delivered laser pulses lasting approximately 100 fs with a tunable central wavelength (720–920 nm) at a repetition rate of 77 MHz. The laser beam was focused onto the Au nanostructure side of the sample at normal incidence using a lens with a focal length of 600 mm. We used this laser for wavelength-dependent PEEM measurements to obtain near-field photoemission (PE) spectra and for near-field mapping at various wavelengths. By changing the irradiation wavelength from 720 nm to 920 nm in 10 nm increments, a series of PEEM images can be obtained. The PE signal from the entire field of view (FOV) can be integrated and plotted against the incidence wavelength; thus, the so-called near-field PE spectra can be obtained. Therefore, near-field properties, such as mapping and spectra, can be investigated *via* this method.

Numerical simulations of the far- and near-field properties of the Au nanostructures investigated in this study were performed using finite-difference time-domain (FDTD) Solutions (Lumerical, Inc.). The ITO-covered glass substrate was assumed to behave as a dielectric material with an average refractive index of $n = 1.55$. The optical properties of Au were obtained using data from Johnson and Christy [32]. The FDTD simulations were performed on a discrete, uniformly spaced mesh with a mesh size of 3 nm.

3. Results and discussion

The mainly metallic NPs investigated in this study were Au dolmen structures. Each dolmen structure consisted of a planar nanorod monomer and a planar nanorod dimer with dimensions of 150 × 100 nm^2 and 80 × 140 nm^2, respectively, as schematically shown in Fig. 1(a). The thickness of the Au dolmen is 30 nm. In the planar nanorod dimer, the edge-to-edge distance between the two nanorods was 70 nm. To guarantee strong interaction between the monomer and the dimer, the gap between the two parts was set to 25 nm. SEM images of the typical dolmen structures are shown in Fig. 1(b), which shows that the dolmen structures have good structural quality. These dolmen structures were arranged in a 2D square array with an area of 100 × 100 μm^2 and a pitch size of 1 μm. The black curve in Fig. 1(c) shows the far-field extinction spectrum under horizontal polarization (*i.e.*, when the electric field vector is perpendicular to the symmetry axis). Since plasmon hybridization occurs only during excitation under horizontally polarized light, in this study, we only investigated the properties under such excitation. Two distinct extinction peaks can be observed in the figure. This observation is consistent with the previously reported far-field optical properties of Au dolmen structures [9, 10, 12]. As we recently reported, the near-field properties of the dolmen structures can be determined using PEEM with femtosecond laser pulses as the excitation source [24]. PEEM can image the electrons emitted from Au nanostructures *via* the multiphoton PE process, especially when the wavelength of the femtosecond laser pulses approaches the LSPR wavelength. Here, the plasmonic local field enhancement leads to the formation of PE intensity distribution on the surface of the Au nanostructures, which enabling the PEEM images to act as nonlinear maps of the near-field intensity distribution of the nanostructures because the PE intensity is nonlinearly correlated with the local near-field intensity. The excitation-wavelength-dependent PEEM measurements using a wavelength-

Optics EXPRESS

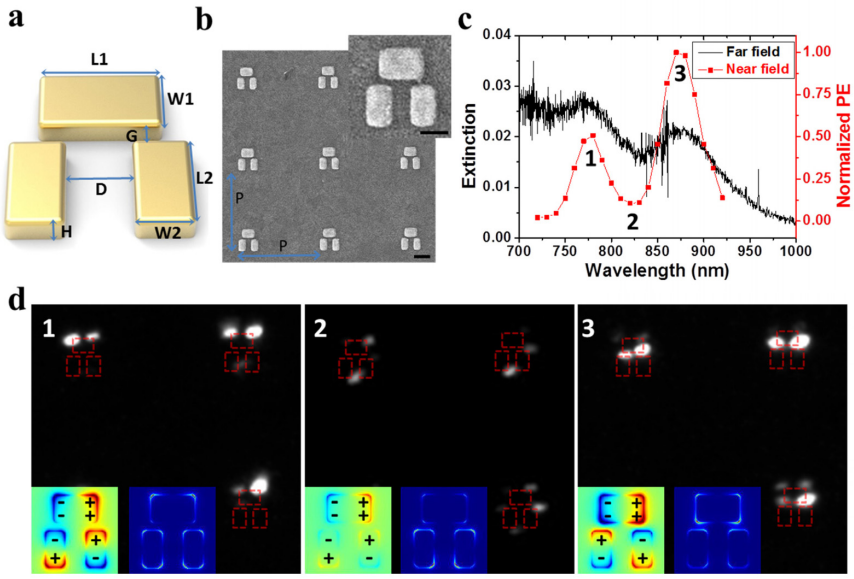

Fig. 1. Far-field and near-field properties of Au dolmen structures. (a) Sketch of an Au dolmen structure that consists of a planar nanorod monomer and a planar nanorod dimer. The design parameters of the structure are as follows: L1 = 150 nm, W1 = 100 nm, G = 25 nm, L2 = 140 nm, W2 = 80 nm, D = 70 nm, and thickness H = 30 nm. (b) SEM image of the Au dolmen structures with the pitch size of 1000 nm. The scale bars are all 200 nm. (c) Experimental far-field extinction spectrum (black) and near-field spectrum (red) of the Au dolmen structures under excitation by horizontally polarized light. (d) PEEM images of a dolmen under the three characteristic excitation wavelengths marked in (c). The red dashed lines represent the geometry of the dolmen structures. The inserts in (d) present the simulated charge distribution (left) and near-field intensity distribution (right) at corresponding excitation wavelengths by FDTD simulations.

tunable femtosecond laser source yielded a near-field PE intensity spectrum that can be regarded as the nonlinear near-field LSPR response spectrum of the plasmonic nanostructures. Using this system, the near-field properties of different kinds of plasmonic nanostructures were investigated [24–26]. In this experiment, we also employed a wavelength-tunable femtosecond laser (720-920 nm) as the excitation source for the PEEM measurements. The setup was the same as it was in our previous investigation [24–26]. A nominal FOV of 10 μm was primarily used in the PEEM measurements. The near-field spectra were obtained by imaging and integrating the near-field PE intensity over the whole FOV at wavelengths ranging from 720 to 920 nm at 10 nm increments. It is worth noting that multiphoton photoemission is considered as the nonlinear photoemission process in our PEEM measurements considering the wavelength range and the laser intensity (50-100 MW/cm^2) [26]. Although the nonlinearity of the photoemission can be varied a little bit within the wavelengths between 720 nm and 920 nm or even at different positions for the same wavelength. An average value of 4 is considered as the nonlinearity, and the measured near-field spectra (wavelength dependent PE intensity spectrum) can be reproduced well by FDTD simulations assuming the constant nonlinearity of 4. The red curve in Fig. 1(c) shows the near-field spectrum of the Au dolmen structures under horizontally polarized light. Two distinct peaks can also be observed, and they located at the position approximately identical to those observed in the far-field spectrum. The two distinct peaks in the far- and near-field spectra resulted from plasmon hybridization between the planar monomers and dimers in the dolmen structures. The peaks correspond to an anti-bonding mode (the shorter-wavelength peak) and a bonding mode (the longer-wavelength peak), as reported in our previous study [24]. Typical PEEM images obtained at these two modes are shown in panels 1 and 3 of Fig.

Optics EXPRESS

1(d); they exhibit different near-field intensity distributions. The redistribution of the near-field enhancement between the upper and lower corners of the monomer is due to the near-field Coulomb interaction between the monomer rod and the dimer rods. Additionally, a PEEM image obtained at the dip wavelength is shown in panel 2 of Fig. 1(d), where notable PE from the dimer rods can be observed. This indicates that a quadrupole mode can be induced in the dimer rods near the dip wavelength, although its contribution to the near-field enhancement is not as pronounced as those of the two hybridized modes. These arguments are also supported by the calculated surface charge distribution and the near-field intensity distribution shown in the insets of Fig. 1(d). In particular, the charge distributions in Panel 1 and 3 of Fig. 1(d) reflect the characters of the anti-bonding and bonding mode, respectively; the calculated near-field intensity distributions also agree well with the PEEM images qualitatively in all the three panels. It is noted that, near the dip wavelength (panel 2 of Fig. 1(d)), the dipole mode in the top monomer part still can be seen, although its contribution to the near-field enhancement significantly decreases. The two hybridized modes and the quadrupole mode have been discussed in detail in our previous study [24].

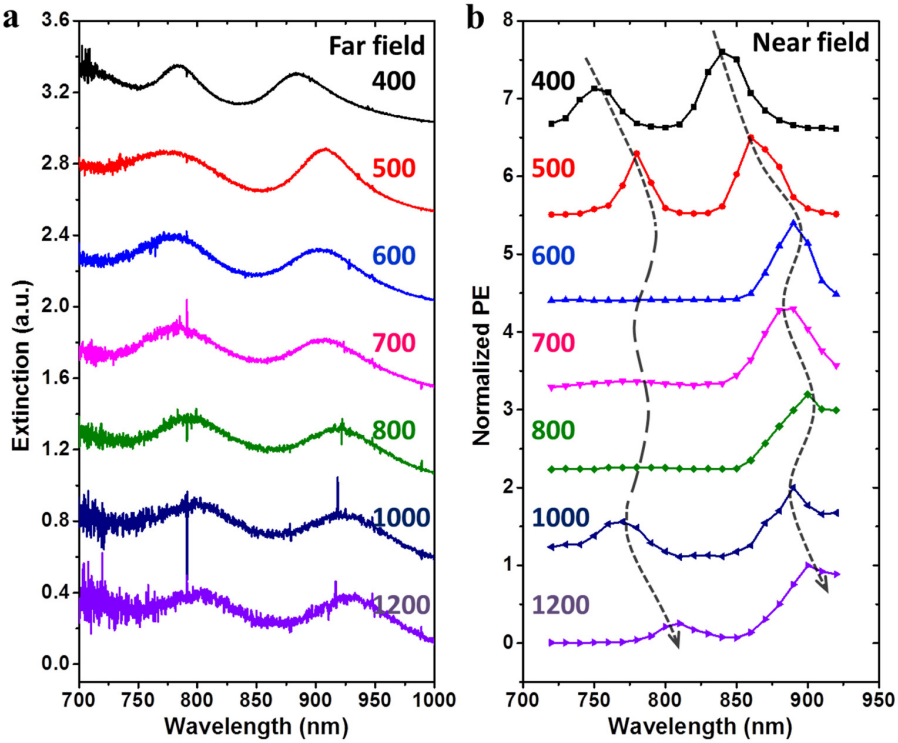

Fig. 2. Experimental far-field and near-field spectra of Au dolmen structures for different pitch sizes. (a) Far-field extinction spectra of Au dolmen structures for 400 nm, 500 nm, 600 nm, 700 nm, 800 nm, 1000 nm, and 1200 nm pitches. For a clear view, each curve is normalized to the extinction strength of the curve for a pitch size of 400 nm in term of the same NP density, and an offset of 0.5 is applied. (b) Near–field spectra of the Au dolmen structures for different pitch sizes obtained using wavelength-dependent PEEM measurements. Each curve is normalized by its maximum photoemission intensity, and an offset of 1 is applied. The black dashed line shows the peak shift tendency as the pitch size varies.

To explore the grating effect in complex Au dolmen structures, we fabricated dolmen structures with pitch sizes ranging from 400 to 1500 nm. The structures with the smallest pitch size (400 nm) were considered large enough to avoid near-field interactions between adjacent units [12]. The experimental far- and near-field spectra are shown in Figs. 2(a) and 2(b), respectively. For a clear view, we present spectra for seven pitch sizes, 400 nm, 500 nm,

Optics EXPRESS

600 nm, 700 nm, 800 nm, 1000 nm, and 1200 nm; arrays with other pitch sizes (450 nm, 550 nm, 650 nm, 900 nm and 1500 nm) were also investigated. In the far-field extinction spectra, the two hybridized plasmon modes localized at approximately 780 nm and 900 nm can be clearly observed for each pitch size. The appearance of the extinction mode at a short wavelength is attributed to the transverse LSPR mode of the dimer rods, which occurred below 700 nm. However, the peak wavelengths of the two hybridized modes were nearly identical for all pitch sizes. In contrast, in the near-field spectra, the two hybridized peaks red shifted first, then blue shifted slightly and red shifted slightly again as the pitch size increased. Such peak shifts can be clearly observed by following the black dashed arrow in Fig. 2(b). These phenomena are similar to the results of previous investigations of the grating effect in plasmonic nanostructures observed through far-field measurements [19, 20]. Furthermore, in our near-field measurements, we found that for some specific pitch sizes (600 nm, 700 nm and 800 nm), the shorter-wavelength peaks became very weak. In other words, the shorter- wavelength peaks were dramatically suppressed with these specific pitch sizes.

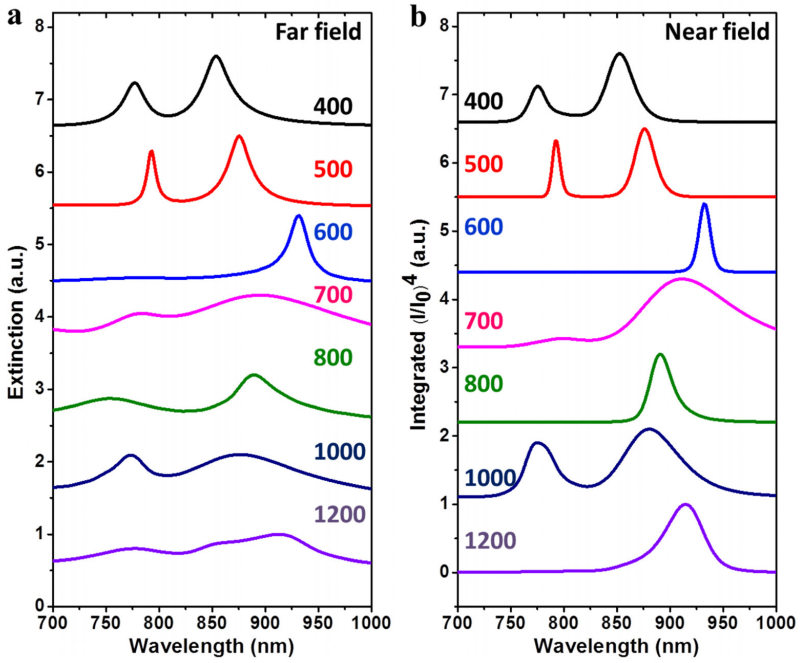

Fig. 3. FDTD simulations of far-field and near-field spectra of Au dolmen structures for different pitch sizes. (a) Simulated far-field spectra of Au dolmen structures for pitch sizes of 400 nm, 500 nm, 600 nm, 700 nm, 800 nm, 1000 nm, and 1200 nm. (b) Simulated near-field spectra of Au dolmen structures with different pitch sizes. The normalized integrated value, $(I/I_0)^4$, over an area of 320 nm × 320 nm at the interface between the dolmen structure and the substrate is shown for better comparison with the PEEM measurements, considering the nonlinearity of the multiphoton photoemission as 4. The simulated far-field and near-field spectra are all normalized by the maximum extinction or PE intensity of each curve, and an offset of 1 is applied.

To understand the differences in the observed optical properties in the near and far fields, we simulated the far- and near-field spectra numerically under light at normal incidence using the FDTD methods as shown in Figs. 3(a) and 3(b), respectively. The results of these simulations for the near-field spectra reproduced our experimental observations qualitatively. Unlike the experimental observations, the dependence of the far-field spectrum on the pitch size was similar to that of the near-field spectrum. However, these results were different from our experimental results. The differences between the experimental results and the numerical

Optics EXPRESS

simulations in the far field are thought to result from the different angles of incidence of the light. In the FT-IR measurements of the far-field spectrum, light was focused on the sample by a Cassegrainian objective lens, which provided angles of incidence between 16° and 32°, whereas in the FDTD simulations, light was irradiated onto the structures at normal incidence. The spectral properties of the plasmonic nanostructures in two regular arrays also depend on the light's angle of incidence. This accounts for the difference in the properties of the far-field spectra in the experiments and the simulations. To verify the influence of the incidence light angle on the far-field spectra, we also simulated the extinction spectra under oblique incidence at 24° (data are not shown). It is found that the LSPR peak wavelengths are less sensitive to the pith size for the oblique incidence compared to those for the normal incidence. It is also noted that the anti-bonding mode at the pitch size of 600 nm can be seen more clearly at the oblique incidence. For the near-field spectra, both the experiments and simulations were performed at normal incidence. Our experimental near-field spectra, simulated far-field spectra and simulated near-field spectra all showed similar dependence of the LSPR wavelength on the pitch size and suppression of the anti-bonding mode (the shorter-wavelength peak) at certain pitch sizes. Notably, the shifts of the two hybridized modes as the pitch size varied were not the same, that is, the anti-bonding mode shifted more slowly than the bonding mode. These interesting phenomena are discussed later.

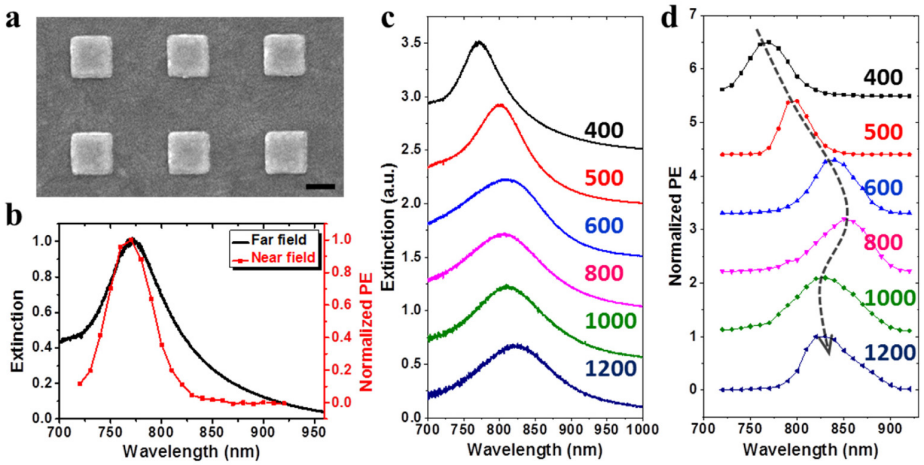

Fig. 4. (a) SEM image of the Au nanoblock structures. The scale bar is 100 nm. (b) Experimental far-field extinction spectrum (black) and near-field spectrum (red) of the Au nanoblocks for a pitch size of 400 nm. Experimental far-field spectra (c) and near-field spectra (d) of Au nanoblocks with different pitch sizes. The black dashed arrow in (d) highlights the peak shift tendency as the pitch size increases.

In dolmen structures, the dipole LSPR mode on the monomer induces the quadrupole mode on the dimers due to near-field interactions, and the quadrupole mode interacts again with the dipole mode resulting in two hybridized plasmon modes (anti-bonding and bonding modes), which dominate the near-field enhancement of the whole dolmen structures. To better understand the grating effect in such complex Au dolmen structures and explain the experimental observations, the far- and near-field spectra of simple Au nanoblock arrays that only generate the simple dipole LSPR mode was investigated for comparison. The Au planer nanoblock structures were 180 × 180 nm^2 in size with a thickness of 30 nm, and the structures were arranged in square lattice arrays with the pitch sizes ranging from 400 to 1500 nm. An SEM image of an array with a pitch size of 400 nm can be found in Fig. 4(a). Figure 4(b) shows the far-field extinction spectrum (black) and the near-field spectrum (red) of the nanoblock array with a pitch size of 400 nm measured using FT-IR spectrometry and PEEM, respectively. The dipole LSPR can be observed at approximately 770 nm in both the far-field

Optics EXPRESS

and the near-field spectra. Far- and near-field spectra for pitch sizes of 400 nm, 500 nm, 600 nm, 800 nm, 1000 nm and 1200 nm are shown in Figs. 4(c) and 4(d), respectively. A slight shift of the plasmon peak wavelength can be observed in the far-field extinction spectra. On contrast, as the pitch size increased, the near-field plasmon peaks first red shifted dramatically, then blue shifted slightly, and finally, red shifted again. Such phenomena can be clearly observed by following the black dashed arrow in Fig. 4(d). In particular, a dramatic red shift emerged when the pitch size increased from 400 nm to 600 nm. This is in good agreement with the previous report on metallic NPs in square lattices; it was previously interpreted as the radiative dipole coupling as *1/d* dependence [19–21]. When the pitch size was larger than 600 nm, some oscillation of the LSPR peak wavelength was observed. We attribute this oscillatory behavior to the grating effect; it was previously reported by Lamprecht *et al.* [19]. It is known that for 2D square gratings of metallic NPs there is a critical pitch size, d_c, at which a new diffractive radiation order emerges for a given wavelength, λ. For normal incidence onto NP arrays on a substrate, there are two values of d_c for first-order diffraction, namely, λ/n and λ, which correspond to radiation onto the substrate (refractive index: n) and into free space, respectively. Near d_c, when the pitch size $d<d_c$, the diffraction is evanescent, and when $d>d_c$, it is radiant. The switch between the evanescent mode and the radiant mode alternates the damping property of the LSPR since the emergence of the new radiant mode increases the radiative loss. The emergence of several values of d_c enable the LSPR peak wavelength to oscillate when the pitch size is larger than the first critical pitch size, λ/n. This behavior has been reported previously based on far-field spectroscopic measurements of simple NP arrays [19, 20, 22]; it was also revealed by our near-field measurements of Au nanoblock arrays. In our experiments, compared to the near-field spectra, the less sensitivity of the plasmon peak wavelength in the far-field spectra to the pitch size is also mainly due to the specific light incidence angles in the FT-IR measurements. More importantly, we found that the peak wavelengths of the two hybridized modes in the dolmen structures were affected by the pitch size in a way similar to that in which the LSPR wavelength in the simple NP arrays is affected in both the experiments and the simulations. This suggests that the anti-bonding and bonding modes are either bright or superradiant since the grating effect for periodic structures is mainly due to interaction between the scattering fields.

To further explore the effect of the grating effect in complex coupled plasmonic systems in the near field, the plasmonic heptamer structures, which have been reported to exhibit Fano resonance by several groups [13, 14, 16, 17], were also considered. In heptamer structures, Fano resonance can arise due to the destructive interference of a spectral wide superradiant mode with a spectral narrow subradiant mode [14, 16]. Halas et al. investigated the near-field properties of Fano resonance in plasmonic heptamer structures using surface-enhanced Raman scattering (SERS) and numerical calculations [13]. They demonstrated that SERS signals are most enhanced when the wavelength of the pump laser and the Raman Stokes mode of interest overlap the Fano dip wavelength. Their results indicate that the subradiant mode dominates the near-field enhancement. In this study, we examined the near-field spectral properties of the Au heptamer structures using PEEM measurements. The heptamer structures investigated in our study comprised circles 140 nm in diameter with gaps of 20 nm between them, which guaranteed strong interaction between the particles. The thickness of the Au nanostructures was also 30 nm. The heptamers were arranged in arrays with pitch sizes ranging from 800 to 1800 nm. Since the entire heptamer structure was large (with dimensions of 460 × 420 nm^2 in the substrate surface plane), the smallest pitch size was set to 800 nm to avoid near-field interaction between two adjacent units. An SEM image of a heptamer array with a pitch size of 1000 nm can be found in Fig. 5(a). Figure 5(b) shows the far-field extinction spectrum (black) and the near-field spectrum (red) of heptamer structures with a pitch size of 1000 nm under excitation by horizontally polarized light. The Fano-like shape can be clearly observed in the far-field extinction spectrum. According to previous reports,

Optics EXPRESS

the dip at a wavelength of 800 nm can be interpreted as the Fano dip [13, 14, 17]. The near-field spectrum shows only one peak, which is located at approximately 780 nm, close to the dip wavelength of the far-field spectrum. The far-field extinction spectra and the near-field spectra of the heptamer arrays with pitch sizes of 800 nm, 900 nm, 1000 nm, 1200 nm, 1500 nm and 1800 nm are shown in Figs. 5(c) and 5(d), respectively. The dip wavelength in far-field spectra are almost constant when varying the pitch size; while in the near-field spectra, each curve shows only one dominant near-field enhancement peak around the far-field spectral dip wavelength. These results indicate that in a heptamer system, the shape of the far-field spectrum is induced by Fano resonance and the subradiant plasmon mode at the Fano resonance dominates the near-field enhancement. Furthermore, the near-field peak wavelengths of the heptamer structures were less sensitive to the pitch size. The observations of plasmonic heptamer structures were different from those of Au nanoblocks and dolmen structures.

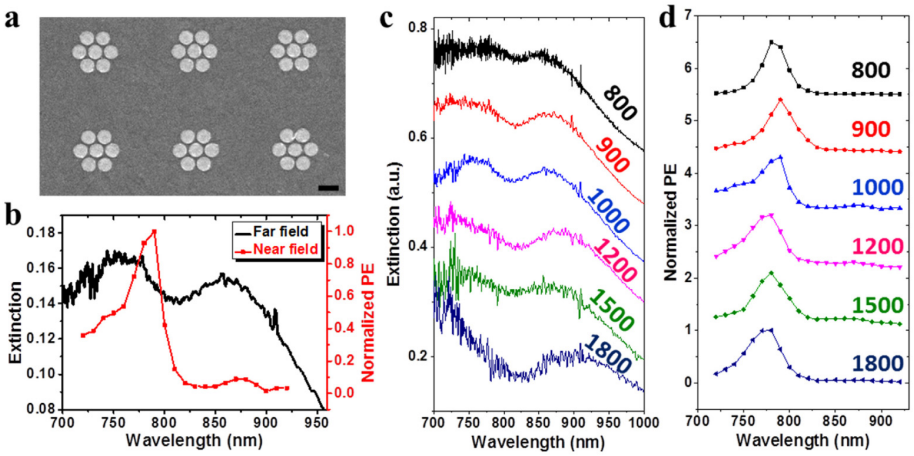

Fig. 5. (a) SEM image of the Au heptamer structures. The scale bar is 200 nm. (b) Experimental far-field extinction spectra (black) and near-field spectra (red) of the Au heptamer structures for a pitch size of 1000 nm. Experimental far-field extinction spectra (c) and near-field spectra (d) of Au heptamer structures with different pitch sizes. In heptamer structures, to avoid near-field interaction between two adjacent units, the smallest pitch size was set to 800 nm. A pitch size of 1800 nm was also investigated.

We investigated the grating effect in plasmonic arrays of dolmen structures, nanoblocks, and heptamer structures using near-field PEEM measurements. For comprehensive comparison, we show the plasmon resonance wavelength as a function of the array's pitch size for different NPs in Figs. 6(a) and 6(b) show the experimentally measured values and the values calculated in the FDTD simulations, respectively. The black and red curves correspond to the hybridized bonding and anti-bonding modes of the dolmen structures, respectively. The green curve represents the dipole resonance mode of the nanoblocks. To create these three curves, we plotted the values for all the pitch sizes we investigated, except for the anti-bonding modes in the dolmen structures. In the case of the anti-bonding modes in the dolmen structures, the resonance mode was suppressed and hard to identify for pitch sizes of 600 nm and 800 nm; therefore, the corresponding data points are missing. The blue curve represents the subradiant mode (corresponding to the near-field enhancement peak wavelength at Fano resonance) in the heptamer structures. For all four resonance modes, there is good agreement between the experiments and the simulations in the dependence of the resonance wavelength on the pitch size. The resonance wavelengths of the two hybridized modes of the dolmen structures and the dipole mode of the nanoblocks exhibited the same dependence on the pitch size, that is, as the pitch size increased, the plasmon modes red shifted dramatically first and then, oscillated. The initial red shift can be contributed to far-field dipole-dipole coupling

Optics EXPRESS

[19–22]. Notably, within the range of pitch size we investigated, there were three maximum wavelengths for each curve. More importantly, the pitch sizes corresponding to these maximum wavelengths were approximately the three critical pitch sizes, namely, the one for first-order grazing diffraction in the substrate, λ/n, the one for first-order grazing diffraction in free space, λ, and the one for second-order grazing diffraction in the substrate, $2\lambda/n$, as indicated by the three dashed lines in Fig. 6(b). From these results, we concluded that for these three plasmon modes, not only the far-field spectra but also the near-field spectra are affected by far-field plasmon coupling and the grating effect [19–22]. However, the resonance wavelengths of near-field plasmon mode observed for the heptamer structures varied only slightly when the pitch size was changed. In particular, no oscillation of the resonance wavelength was observed, even when the pitch size was increased to 1800 nm. This result indicates that this plasmon mode is dominated by absorption rather than scattering; therefore, it is insensitive to the pitch size. Consequently, this mode is further validated as a subradiant or dark mode, which is involved in inducing Fano resonance *via* interaction with a superradiant mode.

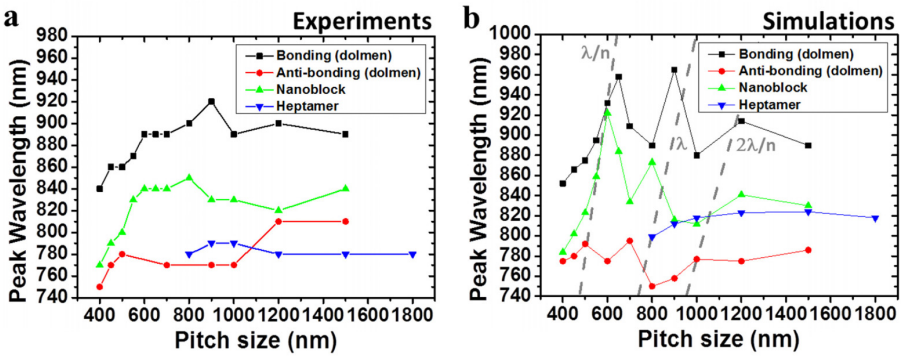

Fig. 6. Near-field peak wavelengths *vs.* pitch sizes for different types of Au nanostructure. (a) Experimental spectrum of near-field peak wavelengths as a function of the pitch size for four plasmon modes in three Au nanostructures, namely, the hybridized bonding mode in dolmens (black), the hybridized anti-bonding mode in dolmens (red), the bright dipole mode in nanoblocks (green), and the subradiant mode in heptamers (blue). In the anti-bonding mode (red curve) for pitch sizes of 600 nm and 800 nm, the resonance mode is suppressed and hard to identify; therefore, the corresponding data points are missing. (b) Numerical simulation results of the plasmon modes in (a). The gray dashed lines show the three modes of the grating effect: first-order grazing diffraction on the substrate, λ/n, first-order grazing diffraction in free space, λ, and second-order grazing diffraction in the substrate, $2\lambda/n$.

Although it is beyond the scope of this paper, the different near-field properties of the dolmen structures and the heptamer structures, which are both typical coupled plasmonic systems, are worth discussing. Previously, we proposed that near-field spectra could be used to reveal the dominant effect (plasmon hybridization or Fano resonance) in near-field enhancement and showed that in dolmen structures, near-field enhancement is dominated by plasmon hybridization rather than Fano resonance. In this study, for the heptamer structures, near-field enhancement exhibited only one main peak located near the dip wavelength in the far-field spectra, which indicates that Fano resonance dominates near-field enhancement. Therefore, we confirm that near-field spectra are very helpful in understanding the plasmon coupling within a coupled plasmonic system in which plasmon hybridization and Fano resonance may be mixed. In this study, the different roles of the grating effect in dolmen and heptamer structures further prove the difference in the near-field properties of these two structures. In dolmen structures, the hybridized anti-bonding and bonding modes dominate the near-field enhancement, but both are superradiant modes and can interact with other dolmen structures within the array through the grating effect. In contrast, in heptamer

Optics EXPRESS

structures, the near-field enhancement is dominated by Fano resonance, which exhibits only very weak far-field coupling and is insensitive to the grating effect.

It is also interesting to evaluate the slight differences in the grating effect between the two hybridized modes of the dolmen structures. Compared to the bonding mode, the anti-bonding mode was dramatically suppressed for certain pitch sizes (especially 600 – 800 nm). For these pitch sizes, the anti-bonding mode seemed to vanish. Actually, the relative strengths between the anti-bonding mode and bonding mode can be tuned by slightly adjusting the geometry of the dolmen. In another group of dolmen arrays, in which the anti-bonding mode was much stronger than the bonding mode in the far-field spectra, we still clearly identified the anti-bonding mode for all pitch sizes, but it was significantly attenuated for pitch sizes between 600 and 800 nm (data are not shown). These attenuations of the anti-bonding mode may be understood based on the formation of this hybridized mode. The anti-bonding mode is generated from the repulsive Coulomb force between the monomers and the dimers, and the maximum near-field enhancement occurs at the two outside corners of the monomer, as shown in Fig. 1(d). This type of anti-bonding mode is unstable compared to the bonding mode; therefore, its intensity may be affected more strongly by the grating effect. Nevertheless, details of the mechanism underlying the attenuation of the anti-bonding mode due to the grating effect need further investigation.

4. Conclusions

In conclusion, we systematically investigated the grating effect for different types of Au nanostructures arranged in 2D square arrays using near-field measurements by PEEM. In particular, the arrays of two coupled plasmonic systems (dolmen and heptamer nanostructures) and one system of individual nanoblocks were studied and compared. Both the two hybridized plasmon modes in the dolmen structures exhibit the dependence of their near-field spectral properties on the pitch size in a manner similar to the dipole mode on the nanoblocks. In all three plasmon modes, as the pitch size increased, the resonance peaks in the near-field spectra were found to first red shift and then, oscillate due to dipole-dipole far-field coupling and the grating effect. In contrast, the grating effect is insignificant in the heptamer structures, where the dark plasmon mode at Fano resonance dominates the near-field enhancement. To our knowledge, this is the first time the grating effect has been investigated in coupled plasmonic nanostructures using near-field measurements. The results demonstrate that different plasmon modes have different sensitivities to the grating effect. This investigation deepens our understanding of far-field coupling and especially the grating effect in complex plasmonic nanostructures and may help with the design and optimization of plasmonic nanostructures for practical applications. We also further validated the applicability of using near-field spectral properties to distinguish the roles of plasmon hybridization and Fano resonances in different coupled plasmonic systems.

Funding

KAKENHI Grant (Nos. JP23225006, JP26870014, JP15H00856, JP15H01073, JP15K04589, and JP15K17438).

Acknowledgments

This study was supported by the Nanotechnology Platform (Hokkaido University), and Dynamic Alliance for Open Innovation Bridging Human, Environment and Materials (Five-Star Alliance) of MEXT.